Fiber Bragg Grating Interrogation and Multiplexing with a 3 × 3 Coupler and a Scanning Filter

Gregg A. Johnson, Michael D. Todd, Bryan L. Althouse, and C. C. Chang

***Abstract*—We present a new technique for fiber Bragg grating (FBG) sensor interrogation and multiplexing. The technique combines a scanning bandpass filter used to multiplex by wavelength multiple gratings in a single fiber, and an unbalanced Mach–Zehnder fiber interferometer made with a 3 × 3 coupler to detect strain-induced wavelength shifts. A demonstration system interrogates four gratings in a single fiber at a sampling rate up to 20 kHz, with a noise floor measured at less than 10 n$\epsilon/\sqrt{\text{Hz}}$ above 0.1 Hz.**

***Index Terms*—Fiber Bragg grating (FBG), interferometry, three-by-three coupler.**

I. Introduction

THE INTRODUCTION of fiber Bragg gratings (FBG's) has launched significant activity in the development of FBG-based sensors and interrogation systems that detect shifts in the center wavelengths of the gratings. The wavelength shifts are caused by axial strains in the lengths of fiber that contain the gratings, which has led to wide application of gratings as strain gages [1]–[5]. Since several FBG's can be written into a single fiber, multiplexing (in addition to bandwidth and sensitivity) is an important consideration in the development of interrogation systems.

The current state-of-the-art wavelength shift systems are based primarily on four designs: scanning Fabry–Perot filter-based interrogation, tunable acousto-optic filter interrogation, wavelength-division-multiplexed (WDM) interferometric interrogation, and prism/CCD-array techniques [6]–[9]. The tunable filter techniques use a broad-band source and broad-band detectors to serially interrogate multiple FBG's in single array by tuning the filter such that a single grating is illuminated at one time. The control voltage applied to the Fabry–Perot filter (or the control frequency applied to the acoustooptic filter) is used to determine the Bragg wavelength of each grating. In the case of the Fabry–Perot filter, the relationship between control voltage and wavelength is not a linear one. The WDM interferometer and CCD-array techniques use a broad-band source and broad-band detectors in conjunction with wavelength separation components to interrogate a number of gratings simultaneously. For the WDM system, the gratings must be centered within the passbands of the WDM filters. Accordingly, large wavelength shifts which move the gratings outside the filter bandwidths can not be tolerated. For this reason, and because very low frequency interrogation of the interferometer is difficult, the WDM system is often used for high frequency, low amplitude measurements. The CCD-array system is much more flexible in its multiplexing capability and can simultaneously sample multiple gratings without confining wavelength shifts to discrete bands.

Comparing systems developed and often deployed by the U.S. Naval Research Laboratory (NRL), the scanning Fabry–Perot filter systems tend to have a low sample rate (<1 kHz) and a noise floor of roughly 100 n$\epsilon/\sqrt{\text{Hz}}$, while the interferometer-based systems have measurement bandwidths up to tens of kilohertz and a noise floor of 5–10 n$\epsilon/\sqrt{\text{Hz}}$ at 100 Hz. Despite lesser bandwidth and sensitivity, the scanning filter design remains popular because it can more easily measure quasi-static strains, and it is much easier to multiplex a high number of FBGs (>10) in a single strand of fiber.

The system described in this paper retains the ease-of-multiplexing nature of the scanning-filter design and the sensitivity of the interferometer-based systems, while surpassing the dynamic range of both systems and the bandwidth of the scanning-filter system, where filter scan rates are typically limited by the design of the electronics. Because it combines the desirable qualities of existing interrogation techniques, it is expected that the present system will be suitable for a broad range of field applications.

II. System Design

The system is sketched in Fig. 1. An array of FBGs is illuminated with a 1550-nm broad-band source (typically, 40-nm bandwidth). Each grating has a Bragg wavelength within the source band, and is separated from the others in wavelength by some application-determined minimum spacing. Ultimately this determines the number of gratings that may be placed in a single array; a typical number is 10–20 gratings. The grating reflection bandwidth is typically less than 0.2 nm, similar to the passband of the scanning filter, ∼0.25 nm. This narrow passband allows the filter to pass a single FBG reflection to the interferometer at a given time. A triangle-wave voltage waveform of appropriate amplitude applied to the scanning filter allows the filter to scan across the entire wavelength range occupied by the gratings.

When the center wavelength of the passband matches an FBG reflection peak, an unbalanced Mach–Zehnder fiber interferometer made with a 3 × 3 coupler is used to determine the strain-induced wavelength shift of the grating. The light intensity at Photodetectors B, C, and D can be used to determine uniquely the relationship between the phase difference ϕ measured across the unbalanced interferometer paths and the grating reflection

Manuscript received January 12, 2000; revised May 2, 2000.

G. A. Johnson, M. D. Todd, and B. L. Althouse are with the Fiber Optic Smart Structures Section, U.S. Naval Research Laboratory, Washington, DC 20375 USA (e-mail: gjohnson@ccs.nrl.navy.mil).

C. C. Chang is with Virginia Polytechnic Institute, Blacksburg, VA 24061 USA.

Publisher Item Identifier S 0733-8724(00)06480-X.

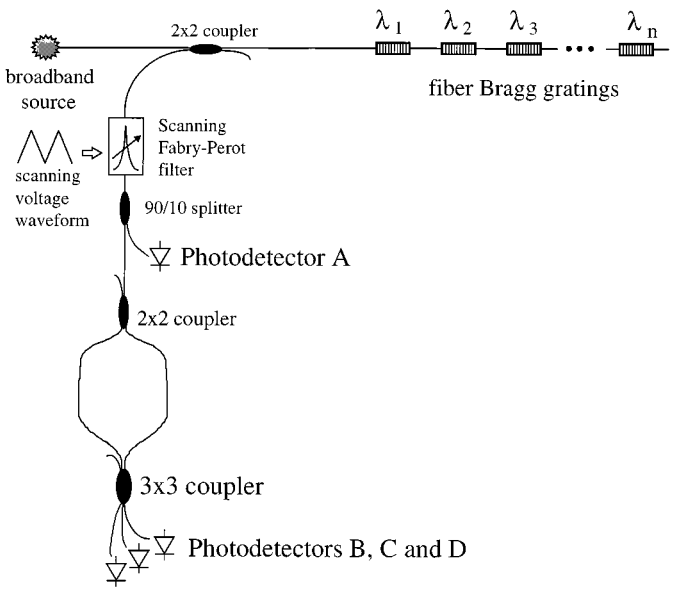

Fig. 1. Bragg grating interrogation system using a scanning bandpass filter and an interferometer containing a 3×3 coupler.

wavelength λ. This general phase/wavelength relationship may be expressed

$$\phi = \frac{2\pi n d}{\lambda} + \phi_0 \tag{1}$$

where

- n is the refractive index of the fiber core;
- d is the difference in length between the interferometer paths;
- λ is the center wavelength of the grating.

The ϕ_0 term is introduced to represent the effects of slowly varying, environmentally induced, random phase shifts due to variations in n and d, typically from temperature fluctuations which occur at time scales assumed significantly longer than signals of interest.

The phase measurement is performed utilizing all three detectors at the outputs of the 3×3 coupler, where the phase is offset 120° ($2\pi/3$ rad) between the three arms. Arbitrarily referencing the measured phase angle to Photodetector B, the photodetector outputs may be expressed as

$$\begin{aligned} V_B &= K_B + G_B \cos\phi \\ V_C &= K_C + G_C \cos(\phi + 2\pi/3) \\ V_D &= K_D + G_D \cos(\phi - 2\pi/3) \end{aligned} \tag{2}$$

where G is the modulation depth of the interferometer and K is the nominal Bragg grating reflection intensity. As the filter passband scans across a grating, the photodetector outputs go through a local maximum indicating that the center wavelengths of the passband and grating coincide. Peak detectors are used to capture the peak voltages of V_B, V_C and V_D, a data acquisition board is triggered to sample the voltages, then the peak detectors are discharged. The three peak voltages are subsequently used to calculate the phase angle ϕ, which in turn is related to the grating wavelength through (1), with effects characterized by ϕ_0 assumed negligible. Strain applied to the gratings, $\Delta\epsilon$, in units of microstrain ($\mu\epsilon$), is determined by changes in the phase angle according to the relation

$$\Delta\epsilon = \frac{\lambda\Delta\phi}{2\pi n d\zeta} \tag{3}$$

which is derived by differentiating (1) with respect to λ and where ζ, given by $(\delta\lambda/\delta\epsilon)/\lambda = 0.74\times10^{-6}\mu\epsilon^{-1}$, relates strain to wavelength shift through photoelastic properties of the fiber. The calculation of strain completes the interrogation of a single grating. The process is repeated as each grating in the array is encountered by the scanning filter.

The method of determining the phase angle from the three outputs of the 3×3 coupler offers some advantages over previous methods [10]–[13]. The method is completely passive, i.e., there is no carrier signal present nor active feedback control, and hence is not bandwidth-limited by active devices. The method is also immune to variations in the source intensity; that is, fluctuations in the intensity of light returned by the gratings are not falsely interpreted as strain. These results are detailed in [14] and summarized here.

From (2) it may be shown that

$$\tan\phi = \frac{\sqrt{3}(\alpha_3 V_C - \alpha_2 V_D)}{(\alpha_3 V_C + \alpha_2 V_D - 2\alpha_2\alpha_3 V_B)} \tag{4}$$

where $\alpha_2 = G_C/G_B = K_C/K_B$ and $\alpha_3 = G_D/G_B = K_D/K_B$. Either source intensity or polarization-induced fluctuations may cause the individual K's and G's to vary, but in the same proportion in each detector. The α terms may be obtained by characterizing the system *a priori* with the application of a known-sized signal.

Because the α terms are insensitive to intensity fluctuations by definition, (4) allows robust recovery of ϕ. An arctangent algorithm with appropriate phase unwrapping may be used for efficient real-time phase extraction. The values $\tan\phi$ and $-\cot\phi$ are obtained by (4) and its negative reciprocal. The arctangent function is then applied to one of these values depending upon $|\tan\phi|$; if $|\tan\phi|$ is less than unity ($|\phi| < \pi/4$), then $\arctan(\tan\phi)$ is calculated; otherwise $-\arctan(\cot\phi)$ is calculated. This result represents the wrapped phase ϕ and is computed in this manner to avoid discontinuities at odd multiples of $\pi/2$ within the unit circle. For unwrapping, a boolean value is tagged simultaneously with the phase computation, and this boolean tag is compared with the previous boolean tag associated with the previous phase computation. If the tags are equal, no phase wrap-around has occurred, and the current phase computation is retained and passed onward. If the tags differ (0 to 1 or 1 to 0), then the current phase computation is incremented or decremented by $\pi/2$, depending on its sign, and passed onward. The entire algorithm is repeated in a while-loop construction until data are no longer being collected.

Fig. 2 is a block diagram of the prototype system for the sampling described above. Photodetector A is used to determine when a grating is being interrogated. As indicated in Fig. 1, Photodetector A gets 10% of the light returning from the grating array prior to insertion into the interferometer. The detector output goes through a local maximum when the scanning filter encounters a grating, and a threshold detector

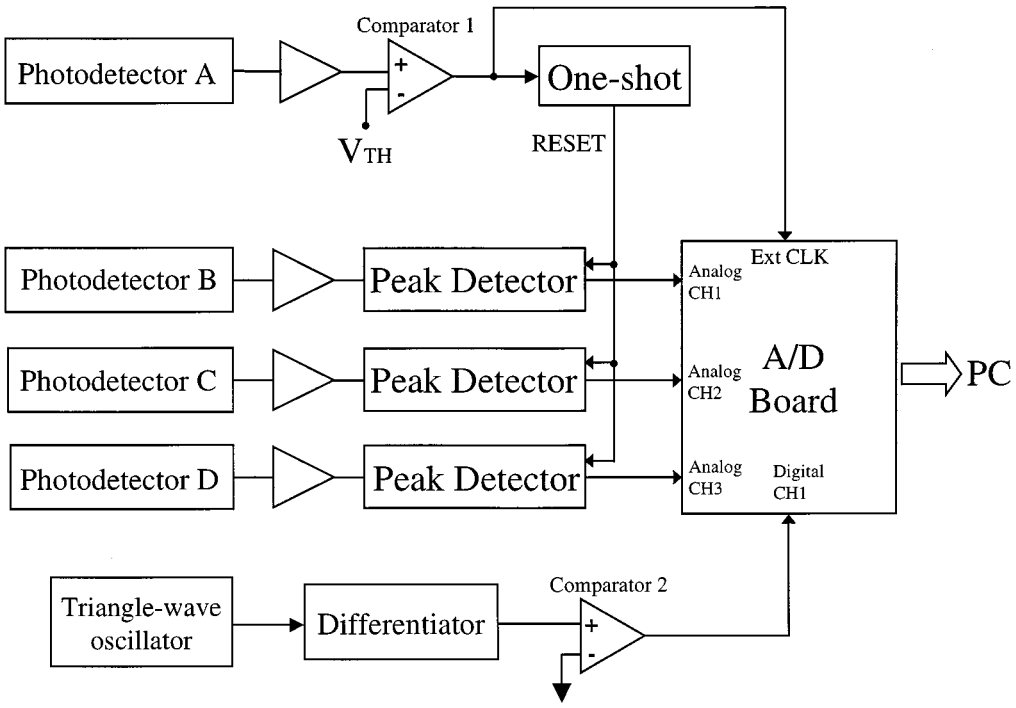

Fig. 2. Block diagram of the prototype system electronics.

(Comparator 1) gives a logic high when a certain amount of light is present (determined by V_{TH}). The falling edge of the comparator output triggers a series of events. By the time of the falling edge, the scanning filter has passed through the peak of the grating reflection, and the peak detectors continue to hold the peak voltages of Photodetectors B–D. The acquisition board is configured to sample on the falling edge of the external clock input, at which time the Peak Detectors are interrogated. The One-shot circuit is also triggered by the falling edge of the comparator, and in turn generates a reset signal that returns the Peak Detector signals to zero volts. At this point, the next grating is ready to be encountered. A differentiator takes the time derivative of the triangle-wave oscillator that drives the scanning filter. The output of the differentiator is a square wave and is used to determine when the filter voltage is increasing or decreasing. Comparator 2 is used to convert the differentiator signal to standard logic levels.

Fig. 3 gives further illustration of the relevant signals. The triangle-wave drive signal and signals from Photodetector A, Comparator 1, the One-shot and one of the three Peak Detectors are shown. The Comparator 1 signal goes high when the threshold voltage is exceeded, indicating that a grating is present. The One-shot signal is triggered by the falling edge of the Comparator 1 signal and is slightly delayed to allow time for the sampling board to sample the Peak Detectors before they are reset. When the One-shot signal goes high, the Peak Detectors are reset to zero.

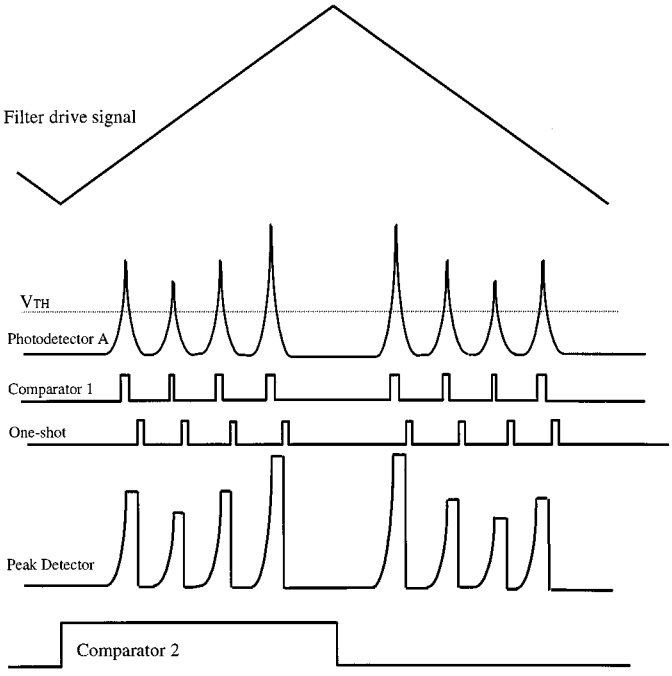

Fig. 3. A timing diagram with the relevant signals for demodulation. The voltage levels of the Peak Detector signals (of which only one of three is shown here) are the measurands used to determine the shifts in wavelength of the Bragg gratings.

III. Experiment

A prototype was constructed and tested to demonstrate the system capabilities. The testing was done with a single array of four Bragg gratings, a Queensgate scanning Fabry–Perot filter, a broad-band source centered about 1550 nm, and a sampling board with 500-kHz sampling capability. The scanning Fabry–Perot filter was driven between 3–10 kHz, resulting in Nyquist sample rates up to 5 kHz. However, the grating arrays could be sampled on both the up- and down-sweep of the filter

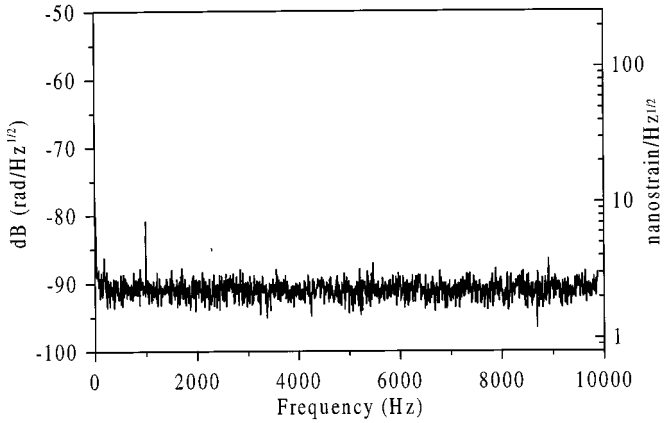

Fig. 4. A noise floor below 5 n$\epsilon/\sqrt{\text{Hz}}$ (on average) is demonstrated for the interrogation system at slightly less than 20 kHz sampling frequency. A sub-microstrain signal at 1 kHz was applied during the test.

drive cycle, resulting in Nyquist sample rates up to 10 kHz. The sensitivity of the phase to changes in grating wavelength (1) is determined in part by the optical path difference in the interferometer, d. In the present system the difference is 2.75 mm, which corresponds to 80.9 microstrain per radian. This path difference was chosen such that the wavelength spacing between fringe maxima occurred at approximately three times the grating bandwidth. The path difference is chosen as large as possible to maintain maximum strain sensitivity but is limited by the coherence length of the grating reflection spectrum, which governs fringe visibility.

A noise floor measurement was performed, and Fig. 4 shows the results in rms radians/$\sqrt{\text{Hz}}$ as well as n$\epsilon/\sqrt{\text{Hz}}$ for the lowest-wavelength grating in the four-grating array. The conversion to microstrain depends on the path imbalance in the interferometer, so it is a more system-specific measurement, while the radian measurement is less dependent on the interferometer. The system with the 2.75-mm path imbalance gives a noise floor of less than 5 n$\epsilon/\sqrt{\text{Hz}}$, which is near $-$90 dB rad/$\sqrt{\text{Hz}}$ or 30 μrad/$\sqrt{\text{Hz}}$. A signal of less than 1 $\mu\epsilon$ peak-to-peak is applied to the Bragg grating under test by bonding it to a piezoelectric transducer driven sinusoidally at 1 kHz.

To demonstrate channel separation, Fig. 5(a) presents the four sensor outputs when a strain signal is applied to one FBG. The signal is applied to the grating by bonding the grating to a 50-cm aluminum beam that is attached in a cantilever fashion to a shaker table and sinusoidally driven at 40 Hz. In this example a 15-microstrain signal is imparted on the sensor placed on the beam, while the other gratings are in the same fiber, but are not attached to the beam.

Finally, a signal was applied to a transducer that modulates the length of one arm of the interferometer. The net result is a 50-Hz signal of peak-to-peak amplitude 6π radians appears on the four sensors, and demonstrates the phase unwrapping capability of the demodulation technique. Fig. 5(b) shows the large signal on each grating, corresponding to equivalent strain levels of 1900 $\mu\epsilon$. Slight offsets are applied to separate the signals for plotting. In both figures, the sampling rate is 3 kS/s.

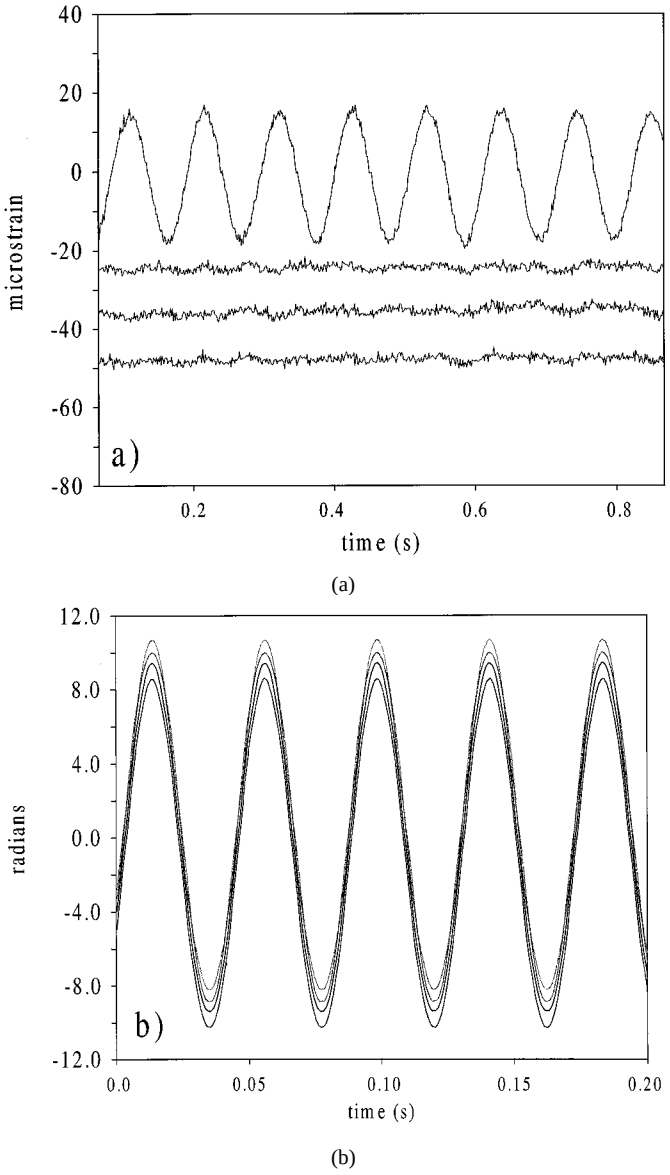

Fig. 5. a) A small strain signal is applied to a single grating of the four-grating array. b) A large signal of 6π radians is applied to all gratings.

As noted in (1), there is an interferometer drift term that affects low-frequency and quasi-static strain measurements. The drift is due to environmental influence on the arms of the fiber interferometer. To combat the low-frequency drift, effort was made to shorten the two arms to 10 cm and to passively stabilize the interferometer temperature with insulation. The results are demonstrated in Fig. 6, showing a 5-n$\epsilon/\sqrt{\text{Hz}}$ (< -80 dB rad/$\sqrt{\text{Hz}}$) spectral density down to 100 mHz.

IV. Conclusion

We have presented a new system for wavelength shift detection of FBG's. The method allows for multiplexing a high number of gratings in a single fiber or multiple fibers. The prototype system demonstrates sampling rates of up to 20 kHz (10 kHz Nyquist) on four gratings in one fiber, frequency-limited in

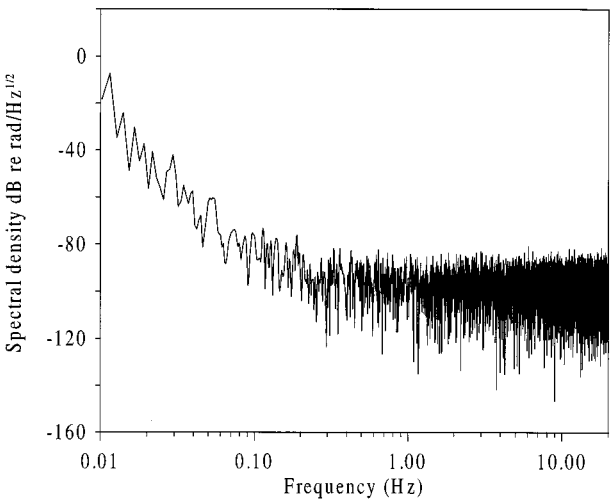

Fig. 6. Low-frequency noise floor.

TABLE I
SUMMARY OF TYPICAL PERFORMANCE CHARACTERISTICS FOR VARIOUS GRATING-BASED INTERROGATION SYSTEM ARCHITECTURES

metric ↓	System Architecture: scanning Fabry-Perot	WDM interferometry	current scheme
dynamic resolution ($n\epsilon/\sqrt{Hz}$)	100	5-10	5
dynamic range (dB)	94	108	114
frequency bandwidth (Hz)	Q[1]-360	100-40,000	Q-20,000
multiplexing capability	16	4-8	>16

[1]"Q" indicates quasi-static.

this case by the scanning filter performance. A passive demodulation scheme utilizing an interferometer made with a 3 × 3 coupler was used, showing a noise floor of 5 $n\epsilon/\sqrt{Hz}$ between 0.1 Hz and 10 kHz. A comparison of demonstrated performance characteristics between the present system and common alternative systems is summarized in Table I.

ACKNOWLEDGMENT

The authors would like to acknowledge technical input from S. T. Vohra, B. Danver, L. Malsawma, and K. Koo.

REFERENCES

[1] A. D. Kersey, M. A. Davis, H. J. Patrick, M. LeBlanc, K. P. Koo, C. B. Askins, M. A. Putnam, and E. J. Friebele, "Fiber grating sensors," *J. Lightwave Technol.*, vol. 15, pp. 1442–1463, 1997.

[2] S. T. Vohra, G. A. Johnson, M. D. Todd, B. A. Danver, and B. L. Althouse, "Distributed strain monitoring with arrays of fiber Bragg grating sensors on an in-construction steel box-girder bridge," *IEICE Trans. Electron.*, vol. E83-C, pp. 454–461, 2000.

[3] G. A. Johnson, K. Pran, G. Wang, G. B. Havsård, and S. T. Vohra, "Structural monitoring of a composite hull air cushion catamaran with a multi-channel fiber Bragg grating sensor system," in *Proc. Structural Health Monitoring Technomic 2000*.

[4] M. D. Todd, G. A. Johnson, and C. C. Chang, "Real-time girder deflection reconstruction using a fiber Bragg grating system," in *Proc. Int. Modal. Analysis. Conf. XVIII*, 2000.

[5] R. Maaskant, T. Alavie, R. M. Measures, G. Tadros, S. H. Rizkalla, and A. Guha-Thakurta, "Fiber-optic Bragg grating sensors for bridge monitoring," *Cement Concrete Composites*, vol. 19, pp. 21–23, 1996.

[6] A. D. Kersey, T. A. Berkoff, and W. W. Morey, "Multiplexed fiber Bragg grating strain-sensor system with a fiber fabry-perot wavelength filter," *Optics Lett.*, vol. 18, pp. 1370–1372, 1993.

[7] H. Geiger, M. G. Xu, N. C. Eaton, and J. P. Dakin, "Electronic tracking system for multiplexed fiber grating sensors," *Electron. Lett.*, vol. 31, pp. 1006–1007, 1995.

[8] A. D. Kersey, T. A. Berkoff, and W. W. Morey, "High resolution fiber Bragg grating based strain sensor with interferometric wavelength detection," *Electron. Lett.*, vol. 28, pp. 236–237, 1992.

[9] C. G. Askins, M. A. Putnam, and E. J. Friebele, "Instrumentation for interrogating many-element fiber Bragg grating arrays embedded in fiber/resin composites," *Proc. SPIE Smart Sensing, Processing Instrum.*, vol. 2444, p. 257, 1995.

[10] K. P. Koo, A. B. Tveten, and A. Dandridge, "Passive stabilization scheme for fiber interferometers using 3 × 3 fiber directional couplers," *Appl. Phys. Lett.*, vol. 40, pp. 616–618, 1982.

[11] Y. Lo, J. S. Sirkis, and C. C. Chang, "Passive signal processing of in-line fiber etalon sensors for high strain-rate loading," *J. Lightwave Technol.*, vol. 15, pp. 1578–1586, 1997.

[12] Y. Lo, "In-fiber bragg grating sensors using interferometric interrogations for passive quadrature signal processing," *IEEE Photon. Technol. Lett.*, vol. 10, pp. 1003–1005, 1998.

[13] I. B. Kwon, M. S. Bae, M. Y. Choi, and H. Moon, "New digital algorithm for determining the direction and magnitude of the strain from quadrature phase-shifted fiber optic signals," in *Proc. SPIE Conf. Sensory Phenomena Measurement Instrum. Smart Structures Mater.*, 1998, pp. 364–375.

[14] M. D. Todd, G. A. Johnson, and C. C. Chang, "Passive, light intensity-independent interferometric method for fibre bragg grating interrogation," *Electron. Lett.*, vol. 35, pp. 1970–1971, 1999.

Gregg A. Johnson received the B.A. degree from Gustavus Adolphus College, St. Peter, MN, in 1990 and the Ph.D. degree in physics from Ohio University, Athens, in 1995.

He is a Research Physicist for the U.S. Navy at the Naval Research Laboratory, Washington, DC. His research interests include measurement instrumentation, fiber optics, and nonlinear dynamics.

Michael D. Todd received the B.S.E., the M.S., and Ph.D. degrees in mechanical engineering from Duke University, Durham, NC, in 1992, 1993, and 1996, respectively.

Since 1996, he has been a Research Engineer with the Fiber Optic Smart Structures section/Optical Sciences division of the U.S. Naval Research Laboratory, Washington, DC, conducting research in fiber-optic transducers, structural dynamics, and nonlinear dynamics.

Bryan L. Althouse received the B.S.E. degree in electrical engineering from Georgia Institute of Technology, Atlanta, GA, in 1997.

Since 1998, he has been with the Fiber Optic Smart Structures section/Optical Sciences Division of the Naval Research Laboratory, Washington, DC, conducting research in fiber-optic sensor/system development and integrated data acquisition systems.

C. C. Chang received the B.S. degree from National Taiwan University, China, in 1986, and the M.S. and Ph.D. degrees from the University of Maryland, College Park, in 1991 and 1996, respectively.

In 1996, he became a Research Associate at Smart Materials and Structures Research Center at University of Maryland. In 1997, he joined the Fiber Optic Smart Structures group at the Naval Research Laboratory, Washington, DC, as a Contracted R&D Engineer. His research interests are in fiber-optic sensors and fiber-optic smart structures.